University of Groningen

Charge transport and trap states in lead sulfide quantum dot field-effect transistors

Nugraha, Mohamad Insan

IMPORTANT NOTE: You are advised to consult the publisher's version (publisher's PDF) if you wish to cite from it. Please check the document version below.

Document Version
Publisher's PDF, also known as Version of record

Publication date:
2017

Link to publication in University of Groningen/UMCG research database

Citation for published version (APA):
Nugraha, M. I. (2017). *Charge transport and trap states in lead sulfide quantum dot field-effect transistors*. [Thesis fully internal (DIV), University of Groningen]. University of Groningen.

Copyright
Other than for strictly personal use, it is not permitted to download or to forward/distribute the text or part of it without the consent of the author(s) and/or copyright holder(s), unless the work is under an open content license (like Creative Commons).

The publication may also be distributed here under the terms of Article 25fa of the Dutch Copyright Act, indicated by the "Taverne" license. More information can be found on the University of Groningen website: https://www.rug.nl/library/open-access/self-archiving-pure/taverne-amendment.

Take-down policy
If you believe that this document breaches copyright please contact us providing details, and we will remove access to the work immediately and investigate your claim.

Downloaded from the University of Groningen/UMCG research database (Pure): http://www.rug.nl/research/portal. For technical reasons the number of authors shown on this cover page is limited to 10 maximum.

Download date: 29-04-2025

Chapter 2

Tunable Doping in PbS Quantum Dot Field-Effect Transistors using Surface Molecular Dipoles

This chapter presents the effect of various self-assembled monolayer (SAM) treatments of the SiO_2 dielectric on the electrical characteristics of PbS quantum dot field-effect transistors (QD-FETs). With the use of SAMs, the threshold voltage of the devices shows a linear relationship with the SAM doping concentration. This study allows tuning the electrical properties of the devices towards n- and p-type doping depending on the type of SAM molecules used. Furthermore, the use of SAMs reduces the interface traps due to the passivation of dangling bonds on the SiO_2 surface. The reduced traps confirm that the threshold voltage shifts and the mobility changes in the devices are attributed to electron/hole doping process and are not caused by the traps induced by the SAMs, as observed in some organic semiconductor systems.

M. I. Nugraha, H. Matsui, S. Z. Bisri, M. Sytnyk, W. Heiss, M. A. Loi, J. Takeya, *APL Mater*. **2016**, *4*, 116105.

2.1 Introduction

Increasing carrier concentration through doping has been used to improve the film conductivity and carrier mobility in different types of semiconductors. This effort has been widely performed in organic field-effect transistors (FETs), whereas doping in colloidal quantum dots (QDs) is generally attempted by using different capping ligands.[1–7] Heavy doping in lead chalcogenide QDs using donor molecules, such as cobaltocene ($CoCp_2$) has also been investigated.[8] Doping with these donor molecules has enabled strong n-type transport in FET devices. However, these heavily-doped PbS QDs result in the FET devices always turned-on with consequent low on/off ratio, which is an undesirable property for some electronic device applications. At this point, light doping of the semiconducting active material is preferred.

Molecular dipoles, well-known as self-assembled monolayers (SAMs), have been widely used to achieve light doping in organic FETs. This light doping is a consequence of band bending due to the modulation of interfacial carrier concentration induced by the SAM molecules. Due to this modulation, the molecules affect the threshold voltage of the devices, allowing the control of charge carrier density as well as the device operation.[9–12] In addition, the use of SAMs can modify the surface properties of the oxide gate dielectric, which influences the morphology of the deposited films. Therefore, the SAM treatment in FETs is very promising to realize high performance devices with controllable operation. These effects have so far been widely studied in organic semiconductors, while the investigation of SAMs in PbS QD-FETs is still limited. In addition, there are still broad types of SAMs that have not been investigated in PbS QD-FETs. This leaves many unsolved questions about the possibility to improve the performance as well as to influence the electrical characteristics of the QD-FETs using SAMs.

In this chapter, we present a study on the effect of SAM surface treatment of the SiO_2 gate dielectric on the electrical characteristics of PbS QD-FETs. Upon the application of SAMs, we observed threshold voltage shifts indicating electron or hole doping introduced by the molecular dipoles on the dielectric surface. We observed an obvious relationship between the threshold voltage of the devices and the doping concentration induced by the SAM molecules, giving us the opportunity to tune the FET properties towards n- or p-type depending on the SAM molecules used. The use of SAMs also allows reducing the density of traps in the devices by passivating the dielectric surface, leading to improved electron mobility up to a factor of three. This light doping strategy through SAM treatment is promising in controlling the electrical characteristics and improving charge carrier mobility in PbS QD-FET devices.

2.2 Doping mechanism using SAMs

In this study, six types of SAM molecules were utilized to functionalize the SiO_2 surface namely hexamethyldisilazane/HMDS, hereinafter referred to as (A), n-octyltriethoxysilane/OTS (B), trimethoxy(2-phenylethyl)silane/PEMS (C), trichlorophenetylsilane/β-PTS (D), 3(mercaptopropyl)trimethoxy-silane/MPMS (E), and dodecylthrichlorosilane/DTS (F). The molecular structures of the SAMs are displayed in Figure 2.1 (a). To ensure that the SAM molecules influence the semiconductor/insulator interface only, a top contact device structure was fabricated as shown in Figure 2.1 (b). In this way, the effect of SAMs on the work function of the source-drain electrodes is minimized. The insertion of the SAM layer between the semiconductor and the dielectric films does not significantly change the total series capacitance due to higher capacitance of the SAM layer than that of the SiO_2 gate dielectric. After the deposition of the semiconductor films on the SiO_2 dielectric, the Fermi level of the semiconductor is aligned with the work function (Fermi level) of the gate electrode as described in Figure 2.1 (c). The treatment of the SiO_2 surface with SAMs introduces dipoles on the surface which allow upward or downward bending of the energy levels of the semiconductor, leading to hole or electron accumulation depending on the polarity of the SAMs. This accumulation of carriers without applying a gate voltage appears as a carrier doping in the devices, which therefore influences the electrical characteristics of the devices.

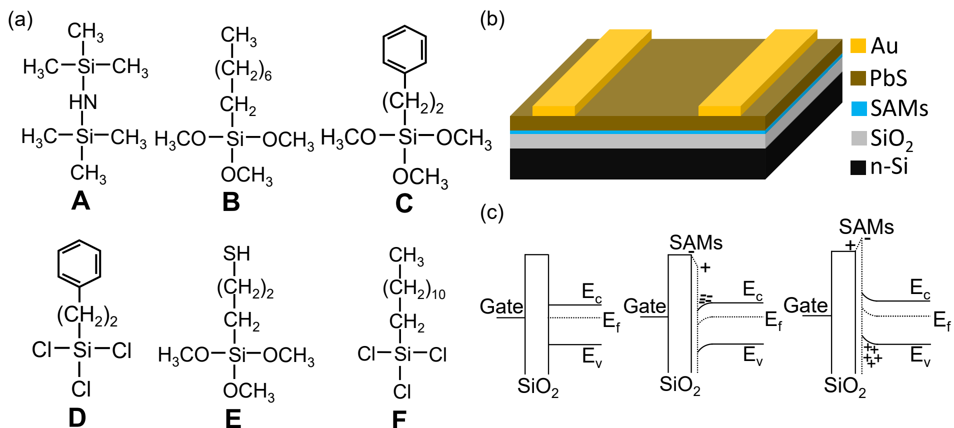

Figure 2.1 (a) Molecular structures of SAMs. (b) Configuration of PbS FETs. (c) Schematic of energy level diagrams in PbS FETs with untreated SiO_2 (left) and SAM-treated SiO_2 (middle and right) at zero gate voltage.

2.3 Properties of PbS films on SAM-treated SiO_2

2.3.1 Morphology of PbS films

As a first step, AFM measurements on PbS films were performed to verify the effect of SAMs on the morphology of the PbS films. Because the first PbS layer has a direct contact with the SAM-treated SiO_2 surface, the AFM images were only taken for this first layer as shown in Figure 2.2 (a)-(f). We found that the use of SAMs on the SiO_2 surface generally promotes a better particle organization as demonstrated by the reduced surface roughness in all films, with the exception of the DTS-treated surface. In DTS-treated SiO_2, the surface becomes very hydrophobic which drastically reduces the wettability of the QD solution in chloroform, producing some particle aggregates during the film deposition.

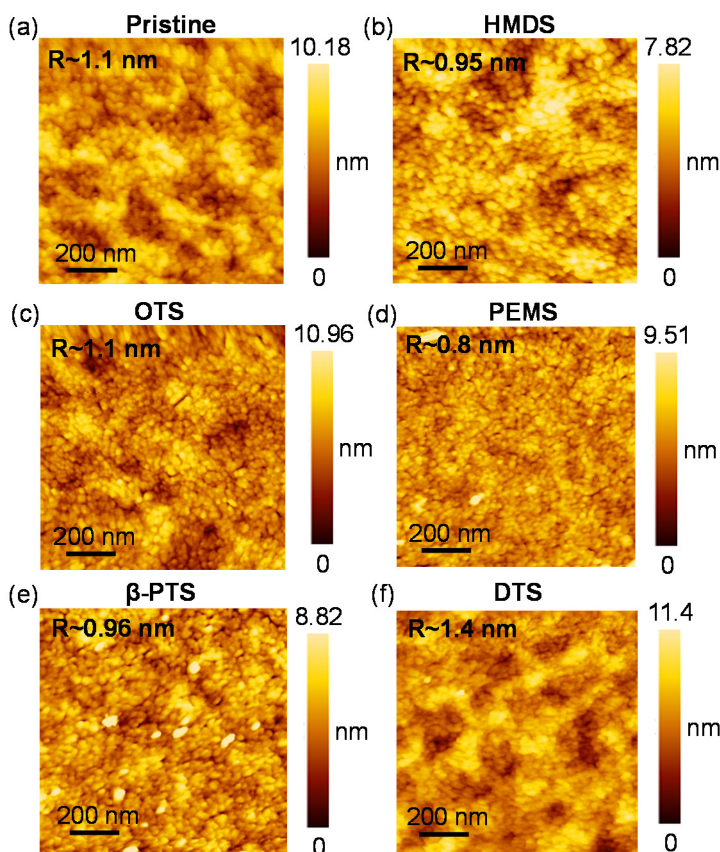

Figure 2.2 AFM images of the first PbS layer on different SAM treated-SiO_2 surfaces with given surface roughness (R).

2.3.2 Electrical Properties of PbS QD-FETs

To investigate the effect of SAM surface treatment of the gate insulator on the electrical characteristics of PbS QD-FETs, we first performed the electrical characterization of the devices without any surface treatment in an N_2-filled glove box. The transfer characteristics of the PbS QD-FETs in the n-channel operation without surface treatment are shown in Figure 2.3 (a). The devices show pronounced n-type properties with extracted electron linear mobility of 0.02 $cm^2V^{-1}s^{-1}$ and a high current modulation of 10^4. The electron mobility is calculated from the forward sweep of the transfer curve, which means that the extracted values do not overestimate the real value of the mobility. In the semi-logarithmic profile of the transfer characteristics, we also observed a slight hole current. Here we focus on the electron transport properties to investigate the effect of SAM surface treatment of the SiO_2 gate dielectric, since the hole current in the devices is much lower than the electron current. The hole transport in the devices is also influenced by the much higher hole trap density with respect to the electron trap density, which may result in uncertainty regarding the effect of doping.[13–15]

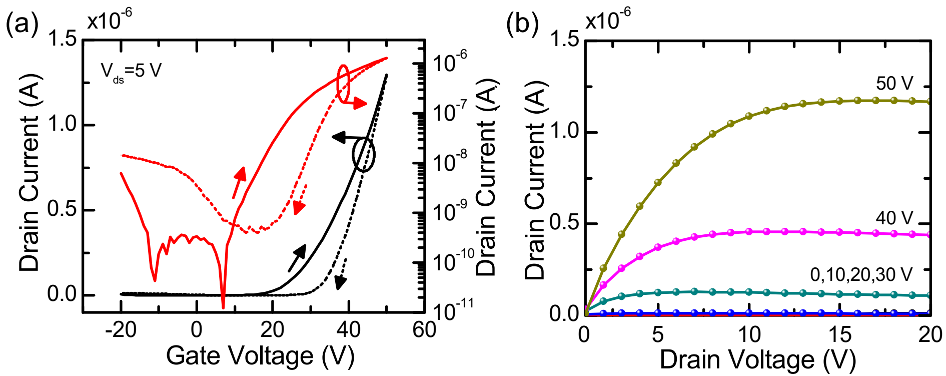

Figure 2.3 (a) I_{ds}-V_g transfer and (b) I_{ds}-V_{ds} output characteristics of pristine PbS FETs.

The FET devices utilize a SiO_2 gate dielectric with thickness of 200 nm defining the oxide capacitance (C_i) of 17.3 nF/cm². By estimating the intercept of the current voltage curve in the x-axis, the threshold voltage of the devices is calculated to be 29 V. To confirm that the devices are in the linear regime at the applied source-drain voltage (V_{ds}), the output characteristics of the devices are displayed in Figure 2.3 (b). From the output characteristics, it is also clear that the devices show both clear linear and saturation regime with no indication of contact limitation.

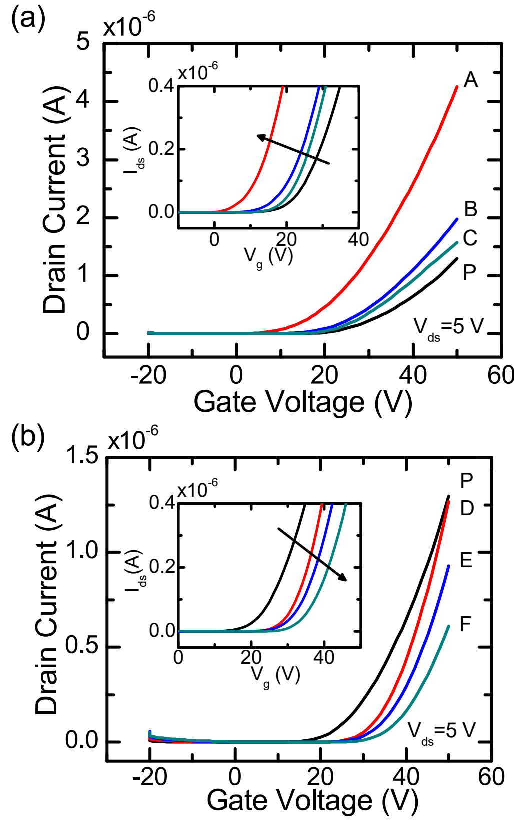

Figure 2.4 I_{ds}-V_g transfer characteristics of PbS FETs after various SAM treatments on the SiO_2 surface indicating (a) electron and (b) hole doping.

The transfer characteristics of PbS QD-FETs on different SAM-treated SiO_2 surfaces are shown in Figure 2.4 (a) and (b). The characteristics of the devices fabricated on the pristine SiO_2 are shown in black line and indicated by 'P'. Using the SAM treatment, we are able to improve as well as to effectively tune the source-drain current of the devices. The treatment of the SiO_2 gate insulator using SAM A shows the highest current and the highest mobility among the tested SAMs. In addition, the SAM surface treatment of the SiO_2 gate dielectric also influences the threshold voltage characteristics of the devices. By treating the SiO_2 surface with SAM A-C, the transfer characteristics shift to negative gate voltages indicating reduced threshold voltage and electron doping in the devices, as demonstrated in Figure 2.4 (a). The inset of Figure 2.4 (a) displays the detailed profiles of the negatively shifted transfer characteristics of the devices with SAM A-C treated SiO_2 dielectric. Conversely, Figure 2.4 (b) shows that the threshold voltage shifts towards more positive voltages when the SiO_2 surface is treated with SAM D-F

indicating hole doping in the devices. A clearer image of the positively shifted transfer characteristics of the devices with SAM D-F treated SiO_2 surface is displayed in the inset of Figure 2.4 (b). With these results, the SAM treatment strategy allows tuning the electrical characteristics of PbS QD-FETs through electron or hole doping, depending on the type of SAM molecules utilized.

2.3.3 SAM doping concentration

At this point, it is interesting to quantify the doping strength induced by the SAM molecules, which corresponds to the concentration of electron and hole doping in the devices. The concentration of electron and hole doping can be estimated from the semi-logarithmic profile of the device transfer characteristics. Figure 2.5 shows the transfer characteristics of PbS QD-FETs in semi-logarithmic scale fabricated on several SAM-treated SiO_2 surfaces. In line with Figure 2.4, a clear shift of the transfer characteristics to negative and positive voltages was demonstrated, depending on the type of SAMs used. In addition, an obvious variation of the on-voltage (V_{on}) of the devices using different SAM treatments was also observed. The V_{on} can be calculated from the gate voltage where the source-drain current starts increasing exponentially. This voltage corresponds to the concentration of electron and hole doping in the devices following the equation $N_{SAMs} = C_i \Delta V_{on} / e$ where ΔV_{on} is the shift of the on-voltage in SAM-treated devices with respect to that in pristine devices.[10] Table 2.1 shows the doping concentration of electron and hole in the devices with different SAM treatments of SiO_2 gate dielectric. The negative values of the doping concentration correspond to electron doping, while the positive values indicate hole doping.

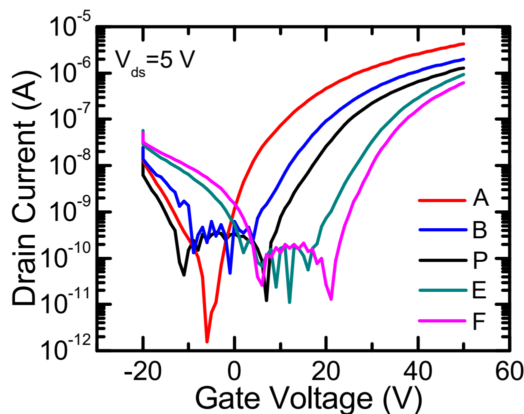

Figure 2.5 I_{ds}-V_g transfer characteristics of PbS FETs in semi-logarithmic scale after various SAM treatments on the SiO_2 surface.

Table 2.1 Carrier doping concentration and trap density in the devices with different SAM treatments.

SAMs	Molecules	N_{SAMs} (10^{12} cm^{-2})	Dipole Moment (D)	N_{traps} (10^{12} eV^{-1} cm^{-2})
P	Pristine	-	-	11.6
A	HMDS	-1.1	-0.98	4.9
B	OTS	-0.54	3.03	10.2
C	PEMS	-0.33	-1.74	9.0
D	β-PTS	0.76	0.41	9.8
E	MPMS	0.97	1.21	10
F	DTS	1.5	0.91	7.4

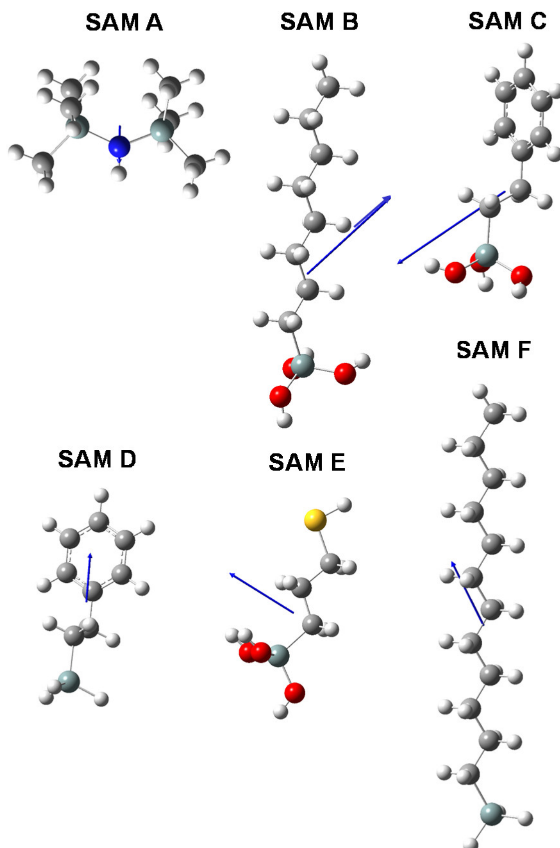

Figure 2.6 Schematic of dipole moments on the SiO_2 surface after treatment with SAM A-F. One of end groups is terminated with H atom to simplify the calculation.

The doping concentration is related to the dipole moments induced by the SAM molecules. The SAM dipole moments and their direction are given in Table 2.1 and displayed in Figure 2.6. These dipole moments are calculated using Gaussian program by terminating the end group of the SAM molecules with hydrogen atom to simplify the calculation. The magnitude and direction of the dipole moments might be influenced by the model used for the calculation using Gaussian program. In Figure 2.6, the negative dipole moments correspond to their downward direction, which favor more electron doping, thus negative concentration values. Meanwhile, upward direction is shown by the positive values of dipole moments which promote hole doping. Interestingly, a peculiar result with SAM B is observed, in which electron doping is produced by a positive dipole moment. In addition, we also did not find a monotonic trend between the magnitude of dipole moment and the number of carrier concentration at a specific type of carrier doping. These results can be attributed to the effective arrangement of the SAM molecules on the SiO_2 surface. It is important to note that the arrangement of the SAMs and their orientation on the SiO_2 surface are very crucial to determine the effective magnitude of dipole moments and the type of charge carrier doping.

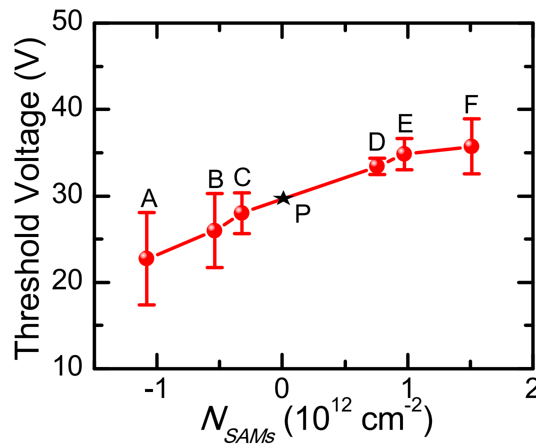

Figure 2.7 The characteristics of threshold voltage for electron accumulation as a function of doping concentration induced by SAMs.

As we compare Figure 2.4 and 2.5, the variation in the V_{on}, thus in doping concentration, is interestingly followed by the threshold voltage shift in the same direction. It further shows that the charges induced by the SAMs are the origin of the shifted transfer characteristics. Figure 2.7 presents a linear relationship between the threshold voltage of the devices and the SAM doping concentration. The deposition of the SAM thin layer builds a series capacitance with respect to

the capacitance of the oxide gate dielectrics (C_i), which induces a threshold voltage shift that can be described as follows,

$$\Delta V_{th} = \frac{C_i + C_{SAMs}}{C_i C_{SAMs}} eN_{SAMs} \approx \frac{eN_{SAMs}}{C_i} \qquad (2.1)$$

where C_{SAMS} and N_{SAMs} are the capacitance of SAMs and the SAM doping concentration, respectively. According to equation (2.1), the inverse gradient of the curve in Figure 2.7 corresponds to the capacitance of the SiO_2 gate dielectric. From Figure 2.7, the calculated gradient of the curve is 5.2 x 10^{-12} V cm^2, which corresponds to the gate dielectric capacitance of 31.1 nF/cm^2. This capacitance value shows a substantial deviation from the one of the actual gate dielectric used in the devices, 17.3 nF/cm^2. This deviation may come from an underestimation of the calculated V_{th}, particularly in the devices with the characteristics shifted towards the right direction, as we refer to Figure 2.4. The V_{th} value can be extracted at different charge carrier densities, which may result in an error in the V_{th} extraction.

2.3.4 Mobility and density of traps

The doping strategy using SAMs also allows determining the charge carrier mobility in the devices. Figure 2.8 (a) displays the electron mobility in the linear regime obtained using different SAM surface treatments. The electron mobility increases with increasing electron doping concentration. We also observed that the electron mobility tends to decrease as the hole doping concentration increases with the exception of the devices treated with SAM D. In this condition, holes in the devices reduce the film conductivity, which result in the decrease of the electron mobility. This could be explained with the recombination of holes and electrons, which gives rise to light emission.[16,17]

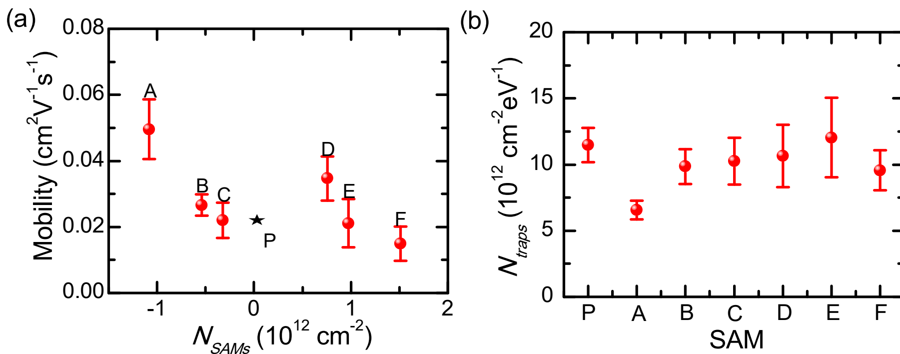

Figure 2.8 (a) Electron mobility as a function of doping density induced by SAMs. (b) The density of traps (N_{traps}) in PbS FETs with various SAM-treated SiO_2 surfaces.

In organic FETs, organosilanes have been indicated to induce additional traps which further reduce the charge carrier mobility.[18,19] Therefore, to confirm that the decrease of the electron mobility is caused by hole doping and not by the additional traps, we quantify the trap density (N_{traps}) in our devices using equation (1.14). The density of traps in the devices using different surface treatments is shown in Figure 2.8 (b) and given in Table 2.1. Obviously, the use of SAMs on the SiO_2 surface reduces the density of electron traps in the devices, which is in agreement with the fact that the SAMs passivate the dangling bonds on the SiO_2 surface. These results further confirm that the decrease of the electron mobility in Figure 2.8 (a), particularly in the devices treated with SAM E and F, originates from the hole doping, not from the SAM-induced traps as observed in some organic FETs.[18,19] In addition, the reduction of the density of traps by almost a factor of three using SAM A contributes to the highest electron mobility in the devices (0.07 $cm^2V^{-1}s^{-1}$). The improvement of the carrier mobility in the devices is not as high as in the case of organic single crystals such as rubrene.[20,21] In rubrene FETs, the trap density in the material is very low. Hence, a small doping level induced by SAMs will have a great impact on the mobility of the charge carriers. Meanwhile, the trap density in PbS FETs is rather high (1.2 x 10^{13} $eV^{-1}cm^{-2}$). Because of this high trap density, the improvement of the mobility in the devices is very reasonable considering the doping level given by the SAMs.

2.4 Conclusion

The effect of various SAM treatments of SiO_2 gate dielectric on the electrical characteristics of PbS QD-FETs has been studied. The use of SAMs resulted in the threshold voltage shifts by inducing electron or hole doping in the devices. The threshold voltage of the devices was found to have a linear relationship with the SAM doping concentration, allowing tuning the electrical characteristics of PbS QD-FETs depending on the type of the SAM molecules used. The use of particular SAMs was also able to improve the electron mobility by a factor of three, which is attributed to higher electron doping as well as lower interface traps than in the devices fabricated on untreated SiO_2 surface. Meanwhile, hole doping results in a decrease of the electron mobility, probably due to the recombination of electron and hole.

2.5 Methods

SAM treatment of SiO_2 dielectric. Heavily n-doped silicon covered with a thermally grown 200 nm thick SiO_2 layer was used as substrates. Before use, the substrates were cleaned with acetone and isopropanol for 10 min, respectively. The substrates were then dried at 120°C to remove residual solvents. Six different

types of SAM molecules, namely, hexamethyldisilazane/HMDS, hereinafter referred to as (A), n-octyltri-ethoxysilane/OTS (B), trimethoxy(2-phenylethyl)silane/PEMS (C), trichloro-phenetylsilane/β-PTS (D), 3-(mercaptopropyl)trimethoxysilane/MPMS (E), and dodecyltrichlorosilane/DTS (F) were used to functionalize the SiO_2 surface. The treatment with SAM A was done by soaking the substrates in SAM A for 1 min followed by spin-coating at 1000 rpm for 1 min (drying). For the treatment with SAM B-E, the substrates were immersed in the corresponding SAM solution (20 μL of SAM molecules in 10 mL of toluene) for 48 h. The last SAM F treatment was done using vapor deposition at atmospheric pressure obtained by placing the SAMs and substrates inside a Teflon container at 120°C for 3 h. To remove the excess of unbound SAM molecules, the substrates were cleaned with acetone and isopropanol for 5 min, respectively. Finally, the substrates were dried at 120°C to remove the residual solvents as well as to promote stronger bonding between the SAM molecules and the SiO_2 surface.

Device fabrication. The deposition of PbS QD films (diameter of 3.6 nm) from 10 mg/mL of oleic acid stabilized-QD solution in chloroform on the previously SAM-treated substrates was done using spin-casting. To improve the conductivity of the films, the long-alkyl chain organic ligands were exchanged with shorter organic molecules, namely 1,2-ethanedithiol (EDT), with concentration of 1% (v/v) in acetonitrile. The film deposition and the ligand exchange (LE) were done using layer-by-layer (LbL) spin-coating method repeated for five times to ensure complete LE process, as previously reported.[22–25] After each LE step, the samples were cleaned with acetonitrile to favor the removal of the exchanged native oleic acid ligands. The devices were then annealed at 120°C for 20 min to remove residual solvents. Finally, Au with thickness of 50 nm was evaporated as source-drain electrode defining the channel length and width of 50 μm and 2 mm, respectively. All device fabrication was performed in an N_2-filled glove box.

Device measurements. The electrical characteristics of FETs were measured using an electrical probe station (placed in an N_2-filled glove box) that is connected to an Agilent B1500A semiconductor parameter analyzer.

2.6 References

[1] M. H. Zarghami, Y. Liu, M. Gibbs, E. Gebremichael, C. Webster, M. Law, *ACS Nano* **2010**, *4*, 2475.

[2] P. R. Brown, D. Kim, R. R. Lunt, N. Zhao, M. G. Bawendi, J. C. Grossman, V. Bulovic, *ACS Nano* **2014**, *8*, 5863.

[3] M. V Kovalenko, M. Scheele, D. V Talapin, *Science* **2009**, *324*, 1417.

[4] D. M. Balazs, D. N. Dirin, H.-H. Fang, L. Protesescu, G. H. ten Brink, B. J. Kooi, M. V. Kovalenko, M. A. Loi, *ACS Nano* **2015**, *9*, 11951.

[5] S. M. Thon, A. H. Ip, O. Voznyy, L. Levina, K. W. Kemp, G. H. Carey, S. Masala, E. H. Sargent, *ACS Nano* **2013**, *7*, 7680.

[6] D. Zhitomirsky, M. Furukawa, J. Tang, P. Stadler, S. Hoogland, O. Voznyy, H. Liu, E. H. Sargent, *Adv. Mater.* **2012**, *24*, 6181.

[7] M. J. Greaney, R. L. Brutchey, *Mater. Today* **2015**, *18*, 31.

[8] W. Koh, A. Y. Koposov, J. T. Stewart, B. N. Pal, I. Robel, J. M. Pietryga, V. I. Klimov, *Sci. Rep.* **2013**, *3*, 2004.

[9] C. Celle, C. Suspène, M. Ternisien, S. Lenfant, D. Guérin, K. Smaali, K. Lmimouni, J. P. Simonato, D. Vuillaume, *Org. Electron.* **2014**, *15*, 729.

[10] K. P. Pernstich, S. Haas, D. Oberhoff, C. Goldmann, D. J. Gundlach, B. Batlogg, A. N. Rashid, G. Schitter, *J. Appl. Phys.* **2004**, *96*, 6431.

[11] J. E. McDermott, M. McDowell, I. G. Hill, J. Hwang, A. Kahn, S. L. Bernasek, J. Schwartz, *J. Phys. Chem. A* **2007**, *111*, 12333.

[12] M. F. Calhoun, J. Sanchez, D. Olaya, M. E. Gershenson, V. Podzorov, *Nat. Mater.* **2008**, *7*, 84.

[13] S. J. Oh, N. E. Berry, J.-H. Choi, E. A. Gaulding, T. Paik, S.-H. Hong, C. B. Murray, C. R. Kagan, *ACS Nano* **2013**, *7*, 2413.

[14] S. J. Oh, N. E. Berry, J.-H. Choi, E. A. Gaulding, H. Lin, T. Paik, B. T. Diroll, S. Muramoto, C. B. Murray, C. R. Kagan, *Nano Lett.* **2014**, *14*, 1559.

[15] M. I. Nugraha, R. Häusermann, S. Z. Bisri, H. Matsui, M. Sytnyk, W. Heiss, J. Takeya, M. A. Loi, *Adv. Mater.* **2015**, *27*, 2107.

[16] C. Rost, S. Karg, W. Riess, M. A. Loi, M. Murgia, M. Muccini, *Appl. Phys. Lett.* **2004**, *85*, 1613.

[17] M. A. Loi, C. Rost-Bietsch, M. Murgia, S. Karg, W. Riess, M. Muccini, *Adv. Funct. Mater.* **2006**, *16*, 41.

[18] K. P. Pernstich, A. N. Rashid, S. Haas, G. Schitter, D. Oberhoff, C. Goldmann, D. J. Gundlach, B. Batlogg, *J. Appl. Phys.* **2004**, *109*, 84510.

[19] S. Kobayashi, T. Nishikawa, T. Takenobu, S. Mori, T. Shimoda, T. Mitani, H. Shimotani, N. Yoshimoto, S. Ogawa, Y. Iwasa, *Nat. Mater.* **2004**, *3*, 317.

[20] J. Takeya, M. Yamagishi, Y. Tominari, R. Hirahara, Y. Nakazawa, T. Nishikawa, T. Kawase, T. Shimoda, S. Ogawa, *Appl. Phys. Lett.* **2007**, *90*, 102120.

[21] J. Takeya, T. Nishikawa, T. Takenobu, S. Kobayashi, Y. Iwasa, T. Mitani, C. Goldmann, C. Krellner, B. Batlogg, *Appl. Phys. Lett.* **2004**, *85*, 5078.

[22] A. G. Shulga, L. Piveteau, S. Z. Bisri, M. V. Kovalenko, M. A. Loi, *Adv. Electron. Mater.* **2016**, *2*, 1500467.

[23] D. M. Balazs, M. I. Nugraha, S. Z. Bisri, M. Sytnyk, W. Heiss, M. A. Loi, *Appl. Phys.*

Lett. **2014**, *104*, 112104.
[24] S. Z. Bisri, C. Piliego, M. Yarema, W. Heiss, M. A. Loi, *Adv. Mater.* **2013**, *25*, 4309.
[25] M. J. Speirs, D. M. Balazs, H.-H. Fang, L.-H. Lai, L. Protesescu, M. V. Kovalenko, M. A. Loi, *J. Mater. Chem. A* **2015**, *3*, 1450.